The bidirectional crosstalk between metastatic uveal melanoma cells and hepatic stellate cells engenders an inflammatory microenvironment

Narjes Babchia, Solange Landreville, Bruno Clement, Cédric Coulouarn,
Frederic Mouriaux

HAL Id: hal-02050392
https://univ-rennes.hal.science/hal-02050392

Submitted on 16 Apr 2019

Title Page

Research Article

Title: The bidirectional crosstalk between metastatic uveal melanoma cells and hepatic stellate cells engenders an inflammatory microenvironment

Authors: Narjes Babchia [a], Solange Landreville[b-e], Bruno Clément[a], Cédric Coulouarn[a,*], Frédéric Mouriaux[a-c,e-f,*]

*CC and FM contributed equally to the work presented here and should therefore be regarded as equivalent senior authors.

Institutional affiliations:

[a] Inserm, Université de Rennes 1, UMR 1241, Nutrition, Métabolismes et Cancer (NuMeCan), Rennes, France

[b] Département d'ophtalmologie, Faculté de médecine, Université Laval, Québec, Canada.

[c] Centre universitaire d'ophtalmologie-Recherche and Axe médecine régénératrice, Centre de recherche du CHU de Québec-Université Laval, Québec, Canada.

[d] Centre de recherche sur le cancer de l'Université Laval, Québec, QC, Canada.

[e] Centre de recherche en organogénèse expérimentale de l'Université Laval/LOEX, Québec, Canada.

[f] Service d'ophtalmologie, CHU de Rennes, Rennes, France.

Corresponding author: Frédéric Mouriaux, UMR 1241 NuMeCan, Pontchaillou University Hospital, 2 rue Henri Le Guilloux, Rennes F-35033, France. Phone: 02 99 28 90 36. Fax: 02 99 28 41 92. Email: Frederic.MOURIAUX@chu-rennes.fr.

Running title: Metastatic uveal melanoma-hepatic stellate cell crosstalk

Word count: 6,155

Total number of figures and tables: 12 Figures (6 in supplements), 5 Supplementary Tables

Abstract

Uveal melanoma is the most common primary ocular neoplasm in adults. It is peculiar for its hematogenous dissemination and its high propensity to spread to the liver. Current treatments rarely prolong patient survival. We hypothesized that metastatic uveal melanoma cells modulate the function of surrounding hepatic stellate cells to facilitate their own growth and survival. This study was conducted to investigate the role of the hepatic microenvironment on uveal melanoma aggressiveness. We demonstrated that the paracrine signaling of surrounding hepatic stellate cells have more transcriptional impact on metastatic uveal melanoma cells. Upregulated transcripts were linked to inflammation and included several interleukins. The uveal melanoma-stellate cell crosstalk induced as well the expression of transmembrane integrins. In addition, the interleukin-6 receptor inhibitor Tocilizumab did not reduce the growth of uveal melanoma cells. Our results provide evidence that inflammatory mediators are key players in the homing of uveal melanoma cells to the liver. The bidirectional crosstalk between uveal melanoma cells and hepatic stellate cells involved pro-fibrogenic interleukins. The inflammatory characteristics of the metastatic microenvironment might offer relevant therapeutic opportunities in uveal melanoma.

1. Introduction

Uveal melanoma (UM) is the most common primary eye tumor in adults, with an estimated annual frequency of 5 to 10 cases per million people in developed countries (Singh et al., 2005). UM is peculiar for its hematogenous dissemination and its high propensity to spread to the liver (Landreville et al., 2008). Current treatments rarely prolong patient survival: the metastasis-related mortality is 20-30% at 5 years and 45% at 15 years (Singh et al., 2011).

The liver is one of the most targeted organs by gastrointestinal and UM metastases, yet the reasons of this tropism remain elusive. Previous studies pointed out to an important role of growth factors mainly synthesized in the liver (HGF/IGF-1) and the expression of corresponding receptors on metastatic UM cells (UMCs; c-MET/IGF-1R) in UM spreading (Barisione et al., 2015; Economou et al., 2008). The microenvironment of the metastasis is an integral part of its physiology and cancer cells need among others surrounding stromal cells for their growth and survival (Mbeunkui and Johann, 2009). Hepatic stellate cells (HSCs) are the most reactive stromal cells of the liver in presence of invading cancer cells (Vidal-Vanaclocha, 2008). Indeed, while they are quiescent cells storing retinoids in healthy liver, they switch into extracellular matrix–producing myofibroblasts when micrometastases develop in the sinusoidal area of lobules (Vidal-Vanaclocha, 2008). Their activation triggers a desmoplastic stromal response that exhibits a pro-invasive effect on colorectal and pancreatic cancer cells, stiffens the extracellular matrix, and suppresses the immune cell infiltration (Yin et al., 2013; Yu et al., 2004). Interestingly, Coupland and collaborators identified that "hepatic fibrosis" and "HSC activation" were among the top-featured pathways found in the UM secretome (Angi et al., 2016). HSCs were previously observed surrounding UM metastases (Grossniklaus, 2013; Lattier et al., 2013), and their conditioned medium increased the migration and invasion of UMCs, as well as their resistance to the MEK inhibitor trametinib (Cheng et al., 2017). In addition, an association between altered inflammatory microenvironment and liver fibrosis was previously suggested (Grossniklaus et al., 2016; Krishna et al., 2017). Grossniklaus and collaborators proposed that the infiltrative growth pattern of UM metastasis, in which malignant lesions are encapsulated by fibrous collagens, was restrained by modifications of the immune microenvironment within the sinusoidal space (Grossniklaus et al., 2016). Coupland and collaborators demonstrated a spatial distribution of CD8-positive tumor infiltrating lymphocytes in metastatic UM, which were predominantly found at the tumor/normal parenchyma interface (Krishna et al., 2017). Activated HSCs and their fibrosis need therefore to be considered as a therapeutic target in the context of combinatorial drug regimens.

The purpose of this study was to investigate the intrinsic differences between primary and metastatic UMCs in their interactions with HSCs. We found that the co-culture of metastatic UMCs with activated HSCs resulted in a bidirectional crosstalk associated with prominent transcriptional changes, and an increase in secretion of inflammatory mediators.

2. Materials and methods

2.1 Cell lines and co-culture experiments

The human LX-2 cell line was kindly provided by Dr. Scott L. Friedman (Mount Sinai School of Medicine, New York, NY) and was maintained as previously described (Xu et al., 2005). The Mel270 cell line was derived from a human primary UM (kindly provided by Dr. Martine Jager, University of Leiden, The Netherlands) (Verbik et al., 1997). The OMM2.3 metastatic cell line was established from a biopsy of a liver nodule from the same patient (Verbik et al., 1997). Both cell lines were grown as previously described (Babchia et al., 2008), and were authenticated using DNA sequencing for *GNAQ* and *GNA11* mutations (positive for *GNAQ Q209P*) and short tandem repeat genotyping (Authentifiler PCR Amplification Kit; Life Technologies) as previously described (Calipel et al., 2011; Mouriaux et al., 2016b). All cell lines were tested routinely for mycoplasma infection by PCR (ATCC). Co-cultures were conducted in serum-free and antibiotic-free DMEM (Invitrogen) using 6-well plates and 1 µm pore-size Transwell inserts (BD Biosciences), which allow the diffusion of soluble factors but prevent cell migration (Supplementary Fig. 1). All cell cultures were maintained at 37°C in a 5% CO_2 atmosphere. Both cell types were then cultured alone or side-by-side for 48 hours (with or without the IL6 receptor inhibitor Tocilizumab (TCZ) at 600 ng/mL diluted directly in serum-free medium). RNA and proteins were then extracted from the cells into the 6-well plates for analysis. Supernatants were collected from inserts for ELISA or used as conditioned medium (CM) for further treatments.

2.2 Microarray analysis

Total RNA was purified from cells at 80% confluence (n=3) with the RNeasy kit (Qiagen). Genome-wide expression profiling was conducted using the low-input Quick Amp Labeling Kit and human SurePrint G3 Human Gene Expression v2 8x60K Microarray Kits (Agilent Technologies). Starting from 150 ng of total RNA, the amplification yield was 7.4 ± 0.94 µg of cRNA and the specific activity was 18.43 ± 3.91 pmol of Cy3 per µg of cRNA. Gene expression data were processed using the Feature Extraction and GeneSpring softwares (Agilent Technologies) and further analyzed using the R-based BRB-Array Tools. Briefly, differentially expressed transcripts were identified by a two-sample univariate *t*-test and a random variance model ($P<0.01$) (Coulouarn et al., 2012). Permutation *P* values for significant transcripts were computed on the basis of 10,000 random permutations.

2.3 Real-Time reverse transcriptase PCR

The expression of relevant transcripts was measured by quantitative real-time PCR (QPCR) using total RNA isolated for the microarray analysis (Coulouarn et al., 2009). Melting analysis was conducted to validate the

specificity of PCR products. Quantitative analysis of PCR data was performed with the $2^{-\Delta\Delta Ct}$ method using beta-Actin (ACTB) and TATA-binding protein (TBP) Ct values for normalization.

2.4 Quantification of cytokines by ELISA

UMC lines were grown as described in Supplementary Fig. 1. Supernatants were collected after 48 hours. The amount of cytokines IL1β, IL6, IL6ST, IL8 and VEGFA secreted in the medium was determined by ELISA using 100 µl of supernatant. The following kit were used: Human IL1β ELISA Kit (Sigma-Aldrich), Human IL6 PicoKine ELISA Kit (Boster Biological Technology), Human sGP130/IL6-ST PicoKine ELISA Kit (Boster Biological Technology), Human IL8/CXCL8 ELISA Kit (Sigma-Aldrich), and Human VEGF DuoSet ELISA (R&D Systems) according to the manufacturer's protocol. The absorbance at 450 nm of the colored solution was quantified with a spectrophotometer (Multiskan Ascent, Thermo), normalized for the number of cells and reported as pg/mL.

2.5 Cell adhesion assay

UMCs and HSCs were resuspended in conditioned medium at 100,000 cells/well, and 150 µL were seeded into a plate precoated with various extracellular matrix proteins (Cell Biolabs; Supplementary Fig. 2). After 90 min, the wells were washed with serum-free DMEM, and 150 µL from each extracted sample was transferred to a 96-well microtiter plate. The absorbance at 560 nm of the colored solution was quantified with a spectrophotometer (Multiskan Ascent, Thermo).

2.6 Cell proliferation

Mel270 and OMM2.3 cell lines were seeded in triplicate in 96-well plates at a density of 10,000 cells/well. Following a 24 hours incubation at 37°C, the medium was replaced by serum-free medium supplemented with 50% (v/v) conditioned medium derived from monocultures or co-cultures of Mel270/LX-2 and OMM2.3/LX-2. UMC and LX-2 cells were seeded in triplicate in 24-well plates at 80% of confluence alone or in co-culture, with or without TCZ. The number of viable cells was determined by using the MTT (3-(4,5- dimethyl thiazol-2-yl)-2,5-diphenyl tetrazolium bromide) colorimetric method after 48 hours of culture. The absorbance at 560 nm was quantified on a spectrophotometer (Multiskan Ascent, Thermo).

2.7 Western blotting

Cells were lysed, resolved, electroblotted (Babchia et al., 2008), and probed with polyclonal antibodies directed against Cyclin D1 (dilution 1:1,000; Cell Signaling Technology), p21 (dilution 1:1,000; Cell Signaling

Technology), STAT3 (dilution 1:1,000; Cell Signaling Technology), and phospho-STAT3 (Tyr705) (dilution 1:1,000; Cell Signaling Technology) to analyze the activation of these kinases in co-culture conditions. Membranes were probed with a rabbit monoclonal antibody directed against the β-Actin (dilution 1:1,000; Santa Cruz Biotechnology) as control for equal loading. Primary antibodies were tagged with specific secondary horseradish peroxidase-conjugated antibodies. Antibody complexes were detected by enhanced chemiluminescence (ECL; Amersham). The intensity of the luminescence was quantified using a charge-coupled device camera combined with an image analysis system (CHEMI-SMART 5000, POMPER150 W; Bioblock Scientific, Fisher).

2.8 Statistical analysis

The two-tailed Student's t-test (normal distribution with equal variance) and the Mann-Whitney U test (nonparametric) were used for statistical analysis. A value of $P<0.05$ was considered to be statistically significant.

3. Results

3.1 Bidirectional crosstalk between UMCs and activated HSCs

We started our study by comparing the morphology and transcriptomic differences between the primary tumor (Mel270; non-metastatic) and metastatic (OMM2.3) UMCs (Supplementary Fig. 3). Our analysis of the transcriptome reveals 256 probes (corresponding to 216 non-redundant well-annotated mRNAs) differentially expressed between Mel270 and OMM2.3 cells (Supplementary Fig. 3B; P<0.01, fold change>1.5). Several transcripts were upregulated in OMM2.3 cells like those associated to extracellular matrix (e.g. MATN4, COL9A1), signaling pathways WNT and BRAF, liver-specific genes (e.g. HNF1A, APOC2), and inflammation (e.g. NFKB, TNFSF10, TNFRSF21, TNFAIP2). We also identified downregulated transcripts in OMM2.3 cells such as CCL20 and CCL3L3. In addition, we observed an elevated secretion of the cytokines IL6ST, IL8 and VEGFA in both cell lines, with higher levels in Mel270 (Supplementary Table 1). Both cytokines IL1β and IL6 were expressed at low levels in UMC lines (Supplementary Fig. 3C). These results demonstrate that there are transcriptomic and secretomic differences between both UMC lines according to their original microenvironment even if they are derived from the same patient. Next, we hypothesized that the exposure of UMC lines to soluble factors produced by activated HSCs may change their phenotype and gene expression profile. Mel270 and OMM2.3 cells were thus co-cultured with LX-2 cells (Supplementary Fig. 1) as a paradigm to study the crosstalk between non-metastatic or metastatic UMCs and activated HSCs. No morphological changes were observed in UMC lines in co-culture conditions (Supplementary Fig. 3A). The analysis of gene expression profiles by means of class comparison allowed identifying 1,200 and 312 transcripts whose expression was modulated significantly in LX-2 cells when co-cultured with metastatic or non-metastatic UMCs, respectively (Fig. 1A). A similar comparison determined that 1,627 and 501 transcripts were significantly modulated by LX-2 cells in metastatic and non-metastatic UMCs, respectively (Fig. 1B). Over 349 transcripts were upregulated and 152 were downregulated in non-metastatic UMCs when co-cultured with LX-2 cells, while 1,013 upregulated transcripts and 614 downregulated transcripts were identified in metastatic UMCs (Supplementary Fig. 4A,C, Supplementary Tables 2-3). Over 747 transcripts were upregulated and 453 were downregulated in LX-2 cells when co-cultured with metastatic UMCs, compared to 252 upregulated transcripts and 60 downregulated transcripts in presence of non-metastatic UMCs (Supplementary Fig. 4B,D, Supplementary Tables 4-5). These results suggest that metastatic UMCs are more responsive to HSCs than non-metastatic UMCs, and conversely. In addition, volcano plots highlighting the significant differences in expressed transcripts in co-culture conditions showed that exposition to LX-2 cells activated three times more transcripts in metastatic UMCs compared to non-metastatic cells (Fig. 1C; P<0.001, fold change>2). Furthermore, metastatic UMCs upregulated fourteen times more transcripts in LX-2 cells than non-metastatic cells (Fig. 1D; P<0.001, fold change>2). According to these microarray results, the number of overexpressed transcripts is twice the number of repressed transcripts, and it thus reveals a bidirectional crosstalk between UMCs and HSCs.

3.2 UMC-HSC crosstalk promotes inflammation

Data mining of genes differentially expressed between monoculture and co-culture conditions demonstrated that inflammation-related genes ranked first (e.g. NFKB pathway), followed by growth factors, signaling pathways such as Notch, and extracellular matrix genes (e.g. collagens, matrix metallopeptidases, integrin receptors). Upregulation of many inflammatory cytokines like IL6, IL6ST and CXCL8 (namely IL8) was observed in all co-culture conditions (Fig. 1C-D). These data indicate that co-culturing UMCs with activated HSCs generates a pro-inflammatory microenvironment. We then validated the microarray data by QPCR. There was a significant upregulation of cytokine transcripts IL1β (5.5-7.5 fold change, $P<0.01$), IL6 (2-10 fold change, $P<0.05$) and IL8 (3-164 fold change, $P<0.01$) in several co-culture conditions (Fig. 2). IL6ST was significantly increased only in the OMM2.3/LX-2 condition (4 fold change, $P<0.001$; Fig. 2B). Again, the response was more pronounced in metastatic UMC-HSC conditions (Fig. 2B,D). Moreover, we confirmed by ELISA the upregulation of corresponding secreted proteins IL6 in both UMC/LX-2 conditions (32-52 fold change, $P<0.001$; Fig. 3A-B), IL6ST in LX-2/UMC conditions (2.5-3 fold change, $P<0.01$; Fig. 3C-D), and IL8 in all co-culture conditions except in the LX-2/Mel270 condition (3-47 fold change, $P<0.001$; Fig. 3). IL1β was expressed at low levels and did not significantly increase in co-culture (Fig. 3). Collectively, these results demonstrate that co-culturing UMCs with activated HSCs induces pro-inflammatory signals. In addition, we observed a significant upregulation of the VEGFA transcript in all co-culture conditions (5-10.5 fold change, $P<0.001$; Fig. 2) and a significant increased of the secreted protein in LX-2/UMC conditions (5-9 fold change, $P<0.001$; Fig. 3), suggesting that the bidirectional crosstalk between UMCs and HSCs generates also a pro-angiogenic microenvironment.

3.3 UMC-HSC crosstalk induces the expression of cell adhesion receptors

Because integrins may play a role in tumor inflammation and growth through their interactions with the extracellular matrix, stromal cells and growth factors, we focused the analysis of our microarray data on integrin subunits (Supplementary Fig. 5A). ITGA5, ITGB2, ITGB3 and ITGB8 were increased in LX-2 cells in co-culture with UMCs (2-21 fold change; Supplementary Fig. 5B), while several were upregulated in metastatic UMCs co-cultured with LX-2 cells (ITGA1, ITGA3, ITGA4, ITGAX, ITGB4; 2-4 fold change; Supplementary Fig. 5C) compared to non-metastatic cells (ITGB3; 2 fold change; Supplementary Fig. 5C). Only ITGA10 was decreased in both UMC lines in co-culture with LX-2 cells (Supplementary Fig. 5C). Therefore, we analyzed the effect of the bidirectional crosstalk on cell adhesion to extracellular matrix proteins such as fibronectin (FN), collagens I or IV (COL I, COL IV), laminin (LN) and fibrinogen (FBG). Interestingly, the Mel270/LX-2 conditioned medium increased the adhesion of Mel270 cells to all extracellular matrix components (>50%; Fig. 4A), while the adhesion of OMM2.3 cells was slightly increased only for FBG (17%; Fig. 4B) when they were incubated with the OMM2.3/LX-2 conditioned medium. The adhesion of LX-2 cells to COL IV and LN was slightly decreased (12 and 17%, respectively; Fig. 4C) when incubated in the LX-2/Mel270 conditioned medium. The LX-2/OMM2.3 conditioned medium did not change their adhesion to any extracellular matrix proteins (Fig. 4D).

These results indicate that co-culturing UMCs with activated HSCs specifically increases the cell adhesion of non-metastatic cells to the extracellular matrix.

3.4 UMC-HSC crosstalk has no effect on cell proliferation

Treatments with the conditioned medium of co-culture conditions had no effect on the proliferation of both UMCs and HSCs as quantified by MTT assays (Fig. 5A). Next, we investigated the mRNA abundance of the proliferation marker MKI67 by QPCR (Fig. 5B). We observed no significant difference in its expression between monocultures and co-culture conditions for all cell lines. Therefore, we analyzed the impact of the bidirectional crosstalk on the levels of cell cycle markers Cyclin D1 (CCND1) and p21 (CDKN1A) by microarray and Western blotting (Fig. 5C,D). The CDKN1A transcript was increased more than two times only in the Mel270/LX2 condition ($P<0.001$; Fig. 5C). Co-culture conditions decreased the protein expression of Cyclin D1 and p21 in UMC lines (Fig. 5D). The Cyclin D1 was barely expressed in LX-2 cells compared to p21 (Fig. 5D). These results indicate that the UMC-HSC crosstalk has no effect on cell proliferation.

3.5 Tocilizumab (TCZ) reduces the inflammation caused by the UMC-HSC crosstalk

Because IL6 was significantly increased in co-culture conditions, we decided to block the binding to its receptor by using TCZ. This humanized anti-human IL6 receptor (IL6R) monoclonal antibody inhibits the binding of both the soluble and membrane-bound forms of the IL6R, leading to the blockade of many biological functions of IL6 (Sato et al., 1993). A growing number of clinical studies have shown the potential use of TCZ to treat inflammatory and autoimmune diseases (Nishimoto et al., 2005). Therefore, we hypothesized that the exposure of UMC-HSC co-cultures to TCZ may reduce the inflammation-induced cytokine expression. We showed by QPCR that the TCZ decreases the expression of the IL6ST transcript in both UMC/LX-2 conditions (54-68%, $P<0.001$; Fig. 6A-B). Maximal inhibition by TCZ was observed with IL1β and to a greater extent in non-metastatic UMCs (59-85%, $P<0.001$; Fig. 6A-B). Minimal inhibition was seen with IL6 in both UMC lines suggesting the presence of an IL6 autocrine loop (17-40%, $P<0.05$; Fig. 6B-D). In addition, there was a decrease in the expression of IL8 (31-57%, $P<0.05$) and VEGFA (43-54%, $P<0.01$) in both UMC/LX-2 conditions (Fig. 6A-B). Because the IL6 binds to the IL6R inducing a homodimerization of the receptor and a subsequent activation of JAK/STAT, ERK and PI3K pathways (Johnson et al., 2012), we hypothesized that the IL6 regulates the inflammation in UMC-HSC co-cultures via the JAK/STAT pathway, and that TCZ should inhibit the activation of STAT3. Indeed, we demonstrated an increase in the phosphorylation of STAT3 in both UMC/LX-2 conditions (Supplementary Fig. 6A). A treatment with TCZ reduced the level of phospho-STAT3 (Supplementary Fig. 6A), suggesting that the IL6 controls the inflammation in UMCs via an activation of STAT3. However, a treatment with TCZ did not have a significant effect on cell proliferation (Supplementary Fig. 6B-D). There was a significant upregulation of

the STAT3 transcript in the OMM2.3/LX2 condition (Supplementary Fig. 6E-F). STAT3 levels were decreased post-TCZ treatment in all co-culture conditions (27-54%, *P*<0.05; Supplementary Fig. 6G-H).

4. Discussion

HSCs are characterized by their expression of key receptors regulating fibrosis such as PDGFRβ, Ob-RL and DDR2, as well as extracellular matrix-remodeling proteins such as MMP-2, TIMP-2, and MT1-MMP (Xu et al., 2005). Their phenotype is considerably heterogeneous *in vivo*, and is likely to reflect the influence of cell-cell communication, including with cancerous cells, as well as their interactions with the extracellular matrix and soluble factors. We used in our study the LX-2 cell line, which greatly recapitulates the *in vivo* phenotype of activated primary hepatic stellate cells (Xu et al., 2005). Its molecular phenotype and activated state was previously validated in our laboratory by microarray (Coulouarn et al., 2012). This cell line thus represents a relevant model to study the bidirectional crosstalk between paired primary and metastatic UMC lines, which are very rare in the field of UM (Calipel et al., 2011; Griewank et al., 2012), and activated stellate cells from the hepatic microenvironment. We showed that in both metastatic co-culture conditions the transcriptional deregulation was more substantial than in non-metastatic UMCs. Our data suggest for the first time that metastatic UMCs are more sensitive to the paracrine signaling of HSCs than non-metastatic UMCs. Their interactions generated a pro-inflammatory, pro-angiogenic and pro-fibrogenic microenvironment.

There is growing evidence that inflammation plays an important role in the initiation phase of UM (Bronkhorst and Jager, 2012), since its genetic instability was associated with an increased number of tumor-infiltrating macrophages and high expression of HLA classes I and II (Bronkhorst and Jager, 2013). However, the literature is scarce concerning the immune microenvironment of metastatic UM (Grossniklaus et al., 2016; Krishna et al., 2017; Qin et al., 2017). In the present study, the co-culture of activated hepatic stellate cells with a pair of UMC lines derived from a primary tumor and its corresponding liver metastasis increased significantly the secretion of pro-inflammatory and pro-fibrogenic interleukins IL6 and IL8. Interestingly, both interleukins were found at high concentrations in the serum of patients with colorectal cancer liver metastases (Ueda et al., 1994), and higher serum levels of IL6 could distinguish patients with primary liver tumors or breast cancer liver metastases from patients with benign liver lesions or without metastasis (Coskun et al., 2004). Moreover, high levels of IL6 were previously associated with poor prognosis in both uveal and cutaneous melanomas (Likhvantseva et al., 1997; Moretti et al., 2001), while high levels of IL8 were linked to increased metastasis in various cancers (Brat et al., 2005; Inoue et al., 2000; Xie, 2001).

Surprisingly, the proliferation of UMC lines was not significantly modified by the paracrine signaling of HSCs. According to clinical experience, some UM patients have metastatic lesions that remain stable during several weeks or months, but then proliferate exponentially and invade the liver (Mouriaux et al., 2016a). Such initial non-proliferation of UMCs may be due to the inhibitory effect of the microenvironment. Here we observed a decrease of Cyclin D1 and p21 proteins in UMC lines co-cultured with HSCs, what may seem contradictory. However, an inverse correlation between the p21 gene expression and evolution from normal skin melanocyte to

11

metastatic melanoma has been previously described (Jiang et al., 1995). It can be explained as a corollary of tumor cells having escaped terminal differentiation and growth arrest by becoming resistant to inhibitory signals from p21 (Mouriaux et al., 1998; Mouriaux et al., 2000). Another possibility is that UMCs exhibit a high level of aggressiveness that is not reflected by a high proliferation rate, but rather by their ability to persist in time in a somewhat hostile environment. Moreover, dynamic adhesion processes are crucial for conferring the migration abilities of cancer cells. For example, metastatic breast cancer cell lines expressed higher levels of integrin subunits than non-metastatic cells (Rizwan et al., 2015). Indeed, several integrins were upregulated in metastatic UMCs co-cultured with activated HSCs, while the cell adhesion to extracellular matrix only increased in non-metastatic cells. It thus suggests that metastatic UMCs retained their adhesive phenotype, a property required to invade a secondary organ. In addition, several integrins act as cell surface receptors for growth factors such as TGFβ (a master regulator of fibrosis), ANGPTL and VEGFA (LaFoya et al., 2018); corresponding transcripts were indeed increased in our co-culture conditions.

IL6-mediated activation of the STAT3 signaling pathway has been shown to regulate cancer cell proliferation, survival, invasion and metastasis (Teng et al., 2014). A growing number of clinical studies have shown the potential use of the IL6 receptor inhibitor TCZ for the treatment of cancer (Nishimoto et al., 2005; Sato et al., 1993). We reported here that the TCZ was a very potent inhibitor of the inflammatory profile showed in UMCs when co-cultured with HSCs. A treatment with TCZ reduced the level of phosphorylated STAT3 in our co-culture conditions, STAT3 being a downstream effector of IL6, which is activated in UMCs exposed to the HSC conditioned medium. However, we did not find any modification of the proliferation of UMCs using such treatment. In fact, anti-IL6 or anti-IL6R monoclonal antibodies have not demonstrated a clinical efficacy in various types of cancer despite evidences showing the involvement of IL6 in controlling the growth of malignant cells and of their healthy counterparts (Rossi et al., 2015). The lack of effect of IL6 inhibitors in cancer is not due to an overproduction of IL6 compared to inflammatory diseases, but rather by the plasticity of tumor cells and the presence of various subclones using growth factors other than this interleukin (Rossi et al., 2015). Finally, it is possible that the IL6 was inadequately suppressed in the microenvironment given the possibility of paracrine, autocrine, and intracrine production by tumor cells, and compensatory effects from other growth factors, which counteract the simple blocking of this cytokine (Ho et al., 2015).

Our findings could potentially benefit immunotherapy of UM. For example, many genes are regulated by the cytokine TGFβ1, which suppresses the immune response by inducing fibrosis and inflammation in aggressive cancers. Ongoing trials for metastatic pancreatic cancer and hepatocellular carcinoma are currently testing in Phase 1 or 2 the TGFβ1 inhibitor Galunisertib in combination with checkpoints inhibitors (Herbertz et al., 2015; https://clinicaltrials.gov, Identifiers# NCT02423343 and NCT02734160).

5. Conclusions

In conclusion, our study demonstrates an increased secretion of inflammatory mediators in UMCs co-cultured with activated HSCs, without an effect on the proliferation of UMCs. Metastatic UMCs were more responsive to the paracrine signaling of HSCs than their non-metastatic counterpart, and conversely. Further investigation of the molecular mechanisms that may explain this discrepancy is underway (e.g. higher expression or sensitivity of the receptors, higher production of soluble factors). A better understanding of the interplay between HSCs and UMCs could be used to discover new therapeutic targets for the metastatic stage such as pro-fibrogenic interleukins.

Acknowledgments

Conflict of interest

The authors declare that there is no conflict of interest regarding the publication of this article.

References

Angi, M., Kalirai, H., Prendergast, S., Simpson, D., Hammond, D.E., Madigan, M.C., Beynon, R.J., Coupland, S.E., 2016. In-depth proteomic profiling of the uveal melanoma secretome. Oncotarget. 7, 49623-49635. https://doi.org/10.18632/oncotarget.10418.

Babchia, N., Calipel, A., Mouriaux, F., Faussat, A.M., Mascarelli, F., 2008. 17-AAG and 17-DMAG-induced inhibition of cell proliferation through B-Raf downregulation in WT B-Raf-expressing uveal melanoma cell lines. Investigative Ophthalmology & Visual Science. 49, 2348-2356. https://doi.org/10.1167/iovs.07-1305.

Barisione, G., Fabbi, M., Gino, A., Queirolo, P., Orgiano, L., Spano, L., Picasso, V., Pfeffer, U., Mosci, C., Jager, M.J., Ferrini, S., Gangemi, R., 2015. Potential Role of Soluble c-Met as a New Candidate Biomarker of Metastatic Uveal Melanoma. JAMA Ophthalmology. 133, 1013-1021. https://doi.org/10.1001/jamaophthalmol.2015.1766.

Brat, D.J., Bellail, A.C., Van Meir, E.G., 2005. The role of interleukin-8 and its receptors in gliomagenesis and tumoral angiogenesis. Neuro-Oncology. 7, 122-133. https://doi.org/10.1215/S1152851704001061.

Bronkhorst, I.H., Jager, M.J., 2012. Uveal melanoma: the inflammatory microenvironment. Journal of Innate Immunity. 4, 454-462. https://doi.org/10.1159/000334576.

Bronkhorst, I.H., Jager, M.J., 2013. Inflammation in uveal melanoma. Eye. 27, 217-223. https://doi.org/10.1038/eye.2012.253.

Calipel, A., Abonnet, V., Nicole, O., Mascarelli, F., Coupland, S.E., Damato, B., Mouriaux, F., 2011. Status of RASSF1A in uveal melanocytes and melanoma cells. Molecular Cancer Research. 9, 1187-1198. https://doi.org/10.1158/1541-7786.MCR-10-0437.

Cheng, H., Chua, V., Liao, C., Purwin, T.J., Terai, M., Kageyama, K., Davies, M.A., Sato, T., Aplin, A.E., 2017. Co-targeting HGF/cMET Signaling with MEK Inhibitors in Metastatic Uveal Melanoma. Molecular Cancer Therapeutics. 16, 516-528. https://doi.org/10.1158/1535-7163.MCT-16-0552.

Coskun, U., Bukan, N., Sancak, B., Gunel, N., Ozenirler, S., Unal, A., Yucel, A., 2004. Serum hepatocyte growth factor and interleukin-6 levels can distinguish patients with primary or metastatic liver tumors from those with benign liver lesions. Neoplasma. 51, 209-213.

Coulouarn, C., Corlu, A., Glaise, D., Guenon, I., Thorgeirsson, S.S., Clement, B., 2012. Hepatocyte-stellate cell cross-talk in the liver engenders a permissive inflammatory microenvironment that drives progression in hepatocellular carcinoma. Cancer Research. 72, 2533-2542. https://doi.org/10.1158/0008-5472.CAN-11-3317.

Coulouarn, C., Factor, V.M., Andersen, J.B., Durkin, M.E., Thorgeirsson, S.S., 2009. Loss of miR-122 expression in liver cancer correlates with suppression of the hepatic phenotype and gain of metastatic properties. Oncogene. 28, 3526-3536. https://doi.org/10.1038/onc.2009.211.

Economou, M.A., All-Ericsson, C., Bykov, V., Girnita, L., Bartolazzi, A., Larsson, O., Seregard, S., 2008. Receptors for the liver synthesized growth factors IGF-1 and HGF/SF in uveal melanoma: intercorrelation

and prognostic implications. Acta Ophthalmology. 86 Thesis 4, 20-25. https://doi.org/10.1111/j.1755-3768.2008.01182.x.

Griewank, K.G., Yu, X., Khalili, J., Sozen, M.M., Stempke-Hale, K., Bernatchez, C., Wardell, S., Bastian, B.C., Woodman, S.E., 2012. Genetic and molecular characterization of uveal melanoma cell lines. Pigment Cell Melanoma Res. 25, 182-187. https://doi.org/10.1111/j.1755-148X.2012.00971.x.

Grossniklaus, H.E., 2013. Progression of ocular melanoma metastasis to the liver: the 2012 Zimmerman lecture. JAMA Ophthalmology. 131, 462-469. https://doi.org/10.1001/jamaophthalmol.2013.2547.

Grossniklaus, H.E., Zhang, Q., You, S., McCarthy, C., Heegaard, S., Coupland, S.E., 2016. Metastatic ocular melanoma to the liver exhibits infiltrative and nodular growth patterns. Hum Pathol. 57, 165-175. https://doi.org/10.1016/j.humpath.2016.07.012.

Herbertz, S., Sawyer, J.S., Stauber, A.J., Gueorguieva, I., Driscoll, K.E., Estrem, S.T., Cleverly, A.L., Desaiah, D., Guba, S.C., Benhadji, K.A., Slapak, C.A., Lahn, M.M., 2015. Clinical development of galunisertib (LY2157299 monohydrate), a small molecule inhibitor of transforming growth factor-beta signaling pathway. Drug Des Devel Ther. 9, 4479-4499. https://doi.org/10.2147/DDDT.S86621.

Ho, L.J., Luo, S.F., Lai, J.H., 2015. Biological effects of interleukin-6: Clinical applications in autoimmune diseases and cancers. Biochemical Pharmacology. 97, 16-26. https://doi.org/10.1016/j.bcp.2015.06.009.

Inoue, K., Slaton, J.W., Kim, S.J., Perrotte, P., Eve, B.Y., Bar-Eli, M., Radinsky, R., Dinney, C.P., 2000. Interleukin 8 expression regulates tumorigenicity and metastasis in human bladder cancer. Cancer Research. 60, 2290-2299.

Jiang, H., Lin, J., Su, Z.Z., Herlyn, M., Kerbel, R.S., Weissman, B.E., Welch, D.R., Fisher, P.B., 1995. The melanoma differentiation-associated gene mda-6, which encodes the cyclin-dependent kinase inhibitor p21, is differentially expressed during growth, differentiation and progression in human melanoma cells. Oncogene. 10, 1855-1864.

Johnson, C., Han, Y., Hughart, N., McCarra, J., Alpini, G., Meng, F., 2012. Interleukin-6 and its receptor, key players in hepatobiliary inflammation and cancer. Translational Gastrointestinal Cancer. 1, 58-70. https://doi.org/10.3978/j.issn.2224-4778.2011.11.02.

Krishna, Y., McCarthy, C., Kalirai, H., Coupland, S.E., 2017. Inflammatory cell infiltrates in advanced metastatic uveal melanoma. Hum Pathol. 66, 159-166. https://doi.org/10.1016/j.humpath.2017.06.005.

LaFoya, B., Munroe, J.A., Miyamoto, A., Detweiler, M.A., Crow, J.J., Gazdik, T., Albig, A.R., 2018. Beyond the Matrix: The Many Non-ECM Ligands for Integrins. Int J Mol Sci. 19. https://doi.org/10.3390/ijms19020449.

Landreville, S., Agapova, O.A., Harbour, J.W., 2008. Emerging insights into the molecular pathogenesis of uveal melanoma. Future Oncology. 4, 629-636. https://doi.org/10.2217/14796694.4.5.629.

Lattier, J.M., Yang, H., Crawford, S., Grossniklaus, H.E., 2013. Host pigment epithelium-derived factor (PEDF) prevents progression of liver metastasis in a mouse model of uveal melanoma. Clinical and Experimental Metastasis. 30, 969-976. https://doi.org/10.1007/s10585-013-9596-3.

Likhvantseva, V.G., Slepova, O.S., Gerasimenko, V.A., 1997. [Interleukin-6 in patients with uveal melanoma]. Vestnik Oftalmologii. 113, 39-41.

Mbeunkui, F., Johann, D.J., Jr., 2009. Cancer and the tumor microenvironment: a review of an essential relationship. Cancer Chemotherapy and Pharmacology. 63, 571-582. https://doi.org/10.1007/s00280-008-0881-9.

Moretti, S., Chiarugi, A., Semplici, F., Salvi, A., De Giorgi, V., Fabbri, P., Mazzoli, S., 2001. Serum imbalance of cytokines in melanoma patients. Melanoma Research. 11, 395-399.

Mouriaux, F., Casagrande, F., Pillaire, M.J., Manenti, S., Malecaze, F., Darbon, J.M., 1998. Differential expression of G1 cyclins and cyclin-dependent kinase inhibitors in normal and transformed melanocytes. Investigative Ophthalmology & Visual Science. 39, 876-884.

Mouriaux, F., Maurage, C.A., Labalette, P., Sablonniere, B., Malecaze, F., Darbon, J.M., 2000. Cyclin-dependent kinase inhibitory protein expression in human choroidal melanoma tumors. Investigative Ophthalmology & Visual Science. 41, 2837-2843.

Mouriaux, F., Servois, V., Parienti, J.J., Lesimple, T., Thyss, A., Dutriaux, C., Neidhart-Berard, E.M., Penel, N., Delcambre, C., Peyro Saint Paul, L., Pham, A.D., Heutte, N., Piperno-Neumann, S., Joly, F., 2016a. Sorafenib in metastatic uveal melanoma: efficacy, toxicity and health-related quality of life in a multicentre phase II study. British Journal of Cancer. 115, 20-24. https://doi.org/10.1038/bjc.2016.119.

Mouriaux, F., Zaniolo, K., Bergeron, M.A., Weidmann, C., De La Fouchardiere, A., Fournier, F., Droit, A., Morcos, M.W., Landreville, S., Guerin, S.L., 2016b. Effects of Long-term Serial Passaging on the Characteristics and Properties of Cell Lines Derived From Uveal Melanoma Primary Tumors. Investigative Ophthalmology & Visual Science. 57, 5288-5301. https://doi.org/10.1167/iovs.16-19317.

Nishimoto, N., Kanakura, Y., Aozasa, K., Johkoh, T., Nakamura, M., Nakano, S., Nakano, N., Ikeda, Y., Sasaki, T., Nishioka, K., Hara, M., Taguchi, H., Kimura, Y., Kato, Y., Asaoku, H., Kumagai, S., Kodama, F., Nakahara, H., Hagihara, K., Yoshizaki, K., Kishimoto, T., 2005. Humanized anti-interleukin-6 receptor antibody treatment of multicentric Castleman disease. Blood. 106, 2627-2632. https://doi.org/10.1182/blood-2004-12-4602.

Qin, Y., Petaccia de Macedo, M., Reuben, A., Forget, M.A., Haymaker, C., Bernatchez, C., Spencer, C.N., Gopalakrishnan, V., Reddy, S., Cooper, Z.A., Fulbright, O.J., Ramachandran, R., Wahl, A., Flores, E., Thorsen, S.T., Tavera, R.J., Conrad, C., Williams, M.D., Tetzlaff, M.T., Wang, W.L., Gombos, D.S., Esmaeli, B., Amaria, R.N., Hwu, P., Wargo, J.A., Lazar, A.J., Patel, S.P., 2017. Parallel profiling of immune infiltrate subsets in uveal melanoma versus cutaneous melanoma unveils similarities and differences: A pilot study. Oncoimmunology. 6, e1321187. https://doi.org/10.1080/2162402X.2017.1321187.

Rizwan, A., Cheng, M., Bhujwalla, Z.M., Krishnamachary, B., Jiang, L., Glunde, K., 2015. Breast cancer cell adhesome and degradome interact to drive metastasis. NPJ Breast Cancer. 1, 15017. https://doi.org/10.1038/npjbcancer.2015.17.

Rossi, J.F., Lu, Z.Y., Jourdan, M., Klein, B., 2015. Interleukin-6 as a therapeutic target. Clinical Cancer Research. 21, 1248-1257. https://doi.org/10.1158/1078-0432.CCR-14-2291.

Sato, K., Tsuchiya, M., Saldanha, J., Koishihara, Y., Ohsugi, Y., Kishimoto, T., Bendig, M.M., 1993. Reshaping a human antibody to inhibit the interleukin 6-dependent tumor cell growth. Cancer Research. 53, 851-856.

Singh, A.D., Bergman, L., Seregard, S., 2005. Uveal melanoma: epidemiologic aspects. Ophthalmology Clinics of North America. 18, 75-84, viii. https://doi.org/10.1016/j.ohc.2004.07.002.

Singh, A.D., Turell, M.E., Topham, A.K., 2011. Uveal melanoma: trends in incidence, treatment, and survival. Ophthalmology. 118, 1881-1885. https://doi.org/10.1016/j.ophtha.2011.01.040.

Teng, Y., Ross, J.L., Cowell, J.K., 2014. The involvement of JAK-STAT3 in cell motility, invasion, and metastasis. JAK-STAT. 3, e28086. https://doi.org/10.4161/jkst.28086.

Ueda, T., Shimada, E., Urakawa, T., 1994. Serum levels of cytokines in patients with colorectal cancer: possible involvement of interleukin-6 and interleukin-8 in hematogenous metastasis. Journal of Gastroenterology. 29, 423-429.

Verbik, D.J., Murray, T.G., Tran, J.M., Ksander, B.R., 1997. Melanomas that develop within the eye inhibit lymphocyte proliferation. International Journal of Cancer. 73, 470-478.

Vidal-Vanaclocha, F., 2008. The prometastatic microenvironment of the liver. Cancer Microenvironment. 1, 113-129. https://doi.org/10.1007/s12307-008-0011-6.

Xie, K., 2001. Interleukin-8 and human cancer biology. Cytokine & Growth Factor Reviews. 12, 375-391.

Xu, L., Hui, A.Y., Albanis, E., Arthur, M.J., O'Byrne, S.M., Blaner, W.S., Mukherjee, P., Friedman, S.L., Eng, F.J., 2005. Human hepatic stellate cell lines, LX-1 and LX-2: new tools for analysis of hepatic fibrosis. Gut. 54, 142-151. https://doi.org/10.1136/gut.2004.042127.

Yin, C., Evason, K.J., Asahina, K., Stainier, D.Y., 2013. Hepatic stellate cells in liver development, regeneration, and cancer. Journal of Clinical Investigation. 123, 1902-1910. https://doi.org/10.1172/JCI66369.

Yu, M.C., Chen, C.H., Liang, X., Wang, L., Gandhi, C.R., Fung, J.J., Lu, L., Qian, S., 2004. Inhibition of T-cell responses by hepatic stellate cells via B7-H1-mediated T-cell apoptosis in mice. Hepatology. 40, 1312-1321. https://doi.org/10.1002/hep.20488.

Figures legends

Fig. 1. Overexpressed transcripts in co-culture were linked to inflammation. **A.** A proportional Venn diagram representing the overlap of deregulated transcripts in OMM2.3/LX-2 (white) and Mel270/LX-2 (black) co-culture conditions. **B.** A proportional Venn diagram representing the overlap of deregulated transcripts in LX-2/OMM2.3 (white) and LX-2/Mel270 (black) co-culture conditions. **C.** Volcano plots (left) demonstrating differentially expressed transcripts in UMC lines grown alone (Mel270, OMM2.3) or co-cultured with HSCs (Mel270/LX-2, OMM2.3/LX-2). Bar graphs (right) showing the expression of cytokines IL1β, IL6, IL6ST, IL8 and VEGFA in these conditions. **D.** Volcano plots (left) demonstrating differentially expressed transcripts in HSCs grown alone (LX-2), in co-culture with Mel270 (LX-2/Mel270) or co-cultured with OMM2.3 (LX-2/OMM2.3). Bar graphs (right) showing the expression of cytokines IL1β, IL6, IL6ST, IL8 and VEGFA in these conditions. Transcripts listed in volcano plots in **C** and **D** were selected on the basis of the significance for their differential expression in monoculture versus co-culture conditions (horizontal dotted lines; $P<0.001$) and the level of induction or repression (vertical dotted lines; fold change>2). Total RNA was extracted after 48 hours and subjected to microarray analysis.

Fig. 2. Quantitative analysis of the expression of cytokine transcripts in co-cultures of UMCs and HSCs. **A-B.** Mel270 and OMM2.3 cells were grown alone or co-cultured with HSCs (Mel270/LX-2; OMM2.3/LX-2). **C-D**. LX-2 cells were grown alone or in co-culture with UMCs (LX-2/Mel270; LX-2/OMM2.3). Total RNA was harvested after 48 hours and the expression of cytokines IL1β, IL6, IL6ST, IL8 and VEGFA was analyzed by QPCR. *$P<0.05$, **$P<0.01$, ***$P<0.001$.

Fig. 3. Quantitative analysis of the production of cytokines in co-cultures of UMCs and HSCs. **A-B**. Mel270 and OMM2.3 cells were grown alone or co-cultured with HSCs (Mel270/LX-2; OMM2.3/LX-2). **C-D.** LX-2 cells were grown alone or in co-culture with UMCs (LX-2/Mel270; LX-2/OMM2.3). Supernatants were collected after 48 hours and the secretion of cytokines IL1β, IL6, IL6ST, IL8 and VEGFA was analyzed by ELISA. *$P<0.05$, **$P<0.01$, ***$P<0.001$.

Fig. 4. Effect of co-culture conditions on cell adhesion of both UMCs and HSCs. **A-B.** Mel270 and OMM2.3 cells were incubated in monoculture conditioned media (Mel270; OMM2.3) or co-culture conditioned media (Mel270/LX-2; OMM2.3/LX-2). **C-D.** LX-2 cells were incubated in monoculture conditioned medium (LX-2) or co-culture conditioned media (LX-2/Mel270; LX-2/OMM2.3). Cells were seeded into plates coated with substrates (extracellular matrix proteins: FN, COL I, COL IV, LN, FBG; negative control: BSA) for 90 min at 100,000 cells/well. Adherent cells were captured, stained and quantified colorimetrically (OD 560 nm).

Fig. 5. Effect of co-culture conditions on cell proliferation of both UMCs and HSCs. **A.** Mel270, OMM2.3 and LX-2 cells were seeded on 96-well plates and treated with conditioned media from monocultures or co-culture conditions. Cell proliferation was measured 24 or 48 hours post-treatment using the MTT colorimetric assay.

B. Total RNA from Mel270, OMM2.3 and LX-2 cells treated with conditioned media from monocultures or co-culture conditions was harvested after 48 hours. The expression of the cell proliferation transcript MKI67 was analyzed by QPCR. **C.** The expression of cell proliferation transcripts CCND1 and CDKN1A was analyzed by microarray. **D.** Total proteins from Mel270, OMM2.3 and LX-2 cells treated with conditioned media from monocultures or co-culture conditions were harvested after 48 hours and the expression of cell proliferation proteins Cyclin D1 and p21 was quantified by Western blotting (β-Actin, control loading). *$P<0.05$, **$P<0.01$, ***$P<0.001$.

Fig. 6. Quantitative analysis of the expression of cytokine transcripts in co-cultures of UMCs and HSCs treated with Tocilizumab (TCZ). **A-B.** Mel270 and OMM2.3 cells were grown in co-culture with HSCs (Mel270/LX-2, OMM2.3/LX-2) or treated with TCZ (Mel270/LX-2 TCZ, OMM2.3/LX-2 TCZ). **C-D.** LX-2 cells were grown in co-culture with UMCs (LX-2/Mel270, LX-2/OMM2.3) or treated with TCZ (LX-2/Mel270 TCZ, LX-2/OMM2.3 TCZ). Total RNA was harvested after 48 hours and the expression of cytokines IL1β, IL6, IL6ST, IL8 and VEGFA was analyzed by QPCR. *$P<0.05$, **$P<0.01$, ***$P<0.001$.

Suppl. Fig. 1. Experimental design of co-cultures of HSCs and UMCs. **A-B.** LX-2 cells (HSCs) were seeded onto cell culture inserts with 1 µm pore size (upper chamber) and were loaded into 6-well receiver plates containing UMC lines Mel270 (**A**) or OMM2.3 (**B**). This pore size allows the diffusion of secreted components in the medium but prevents cell migration toward the lower chamber. **C-D.** Mel270 or OMM2.3 cells were seeded onto cell culture inserts (upper chamber) and were loaded into 6-well receiver plates containing LX-2 cells. HSCs and UMCs were cultured alone or side-by-side for 48 hours, and then RNA and proteins were extracted from the cells and subjected to microarray analyses and Western blotting. Supernatants were collected from inserts to perform ELISA analyses or used later as conditioned medium (CM).
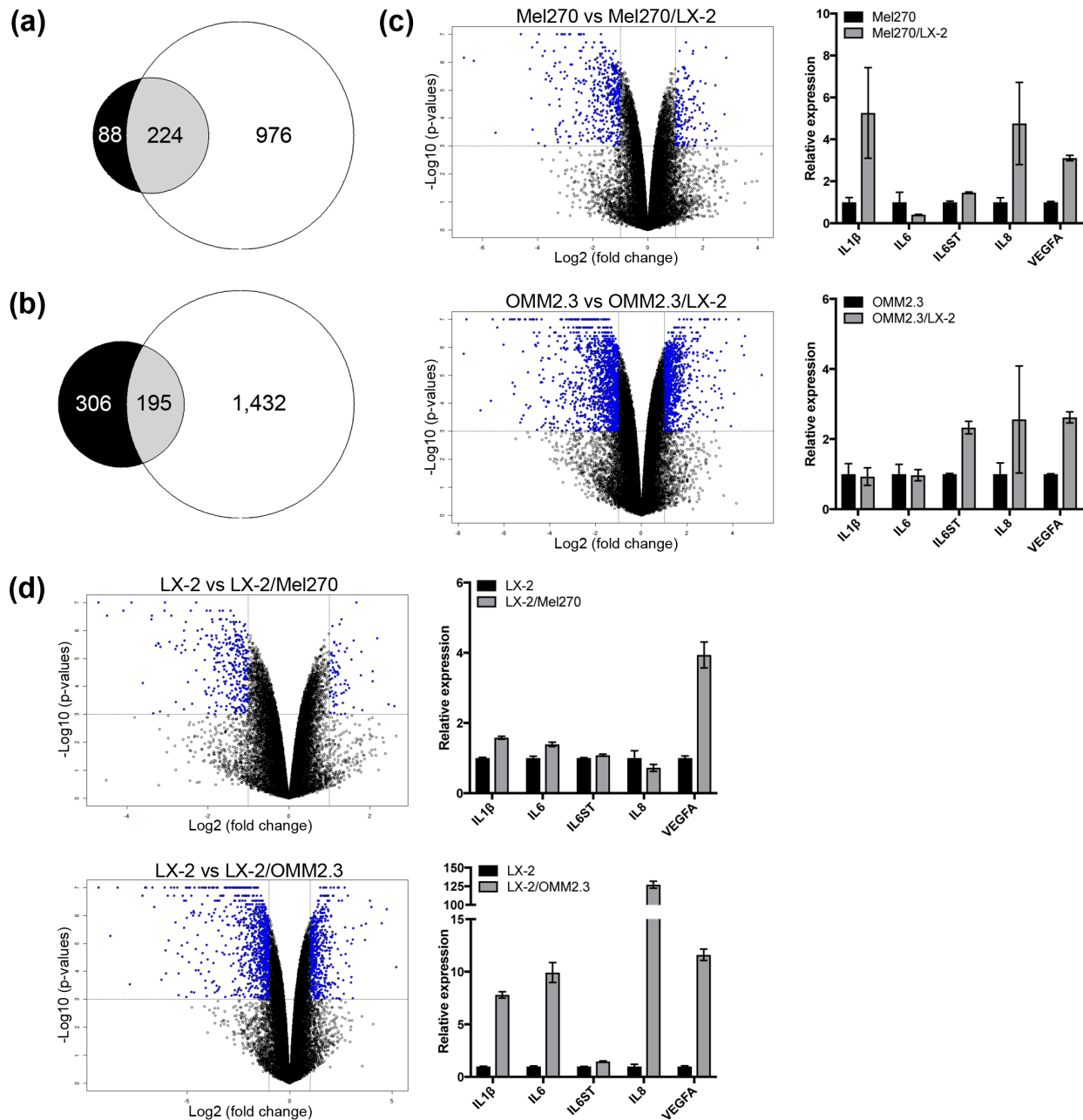
Suppl. Fig. 2. Extracellular matrix array. Adherent cells were stained and quantified colorimetrically after 90 min of incubation (purple; OD 560 nm). Extracellular matrix proteins: FN, COL I, COL IV, LN, FBG; negative control: BSA.
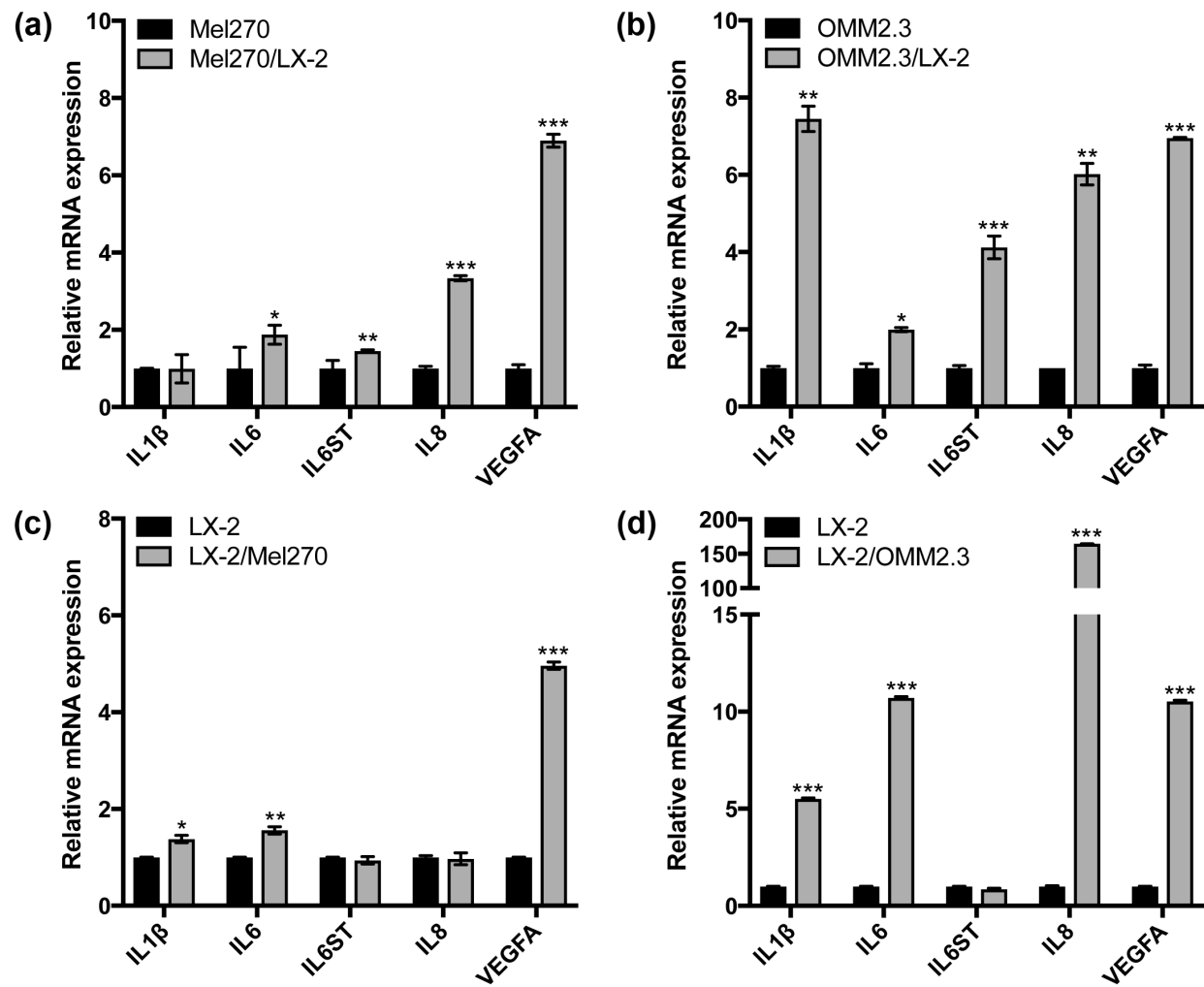
Suppl. Fig. 3. Comparison between UMC lines grown alone. **A.** Typical spindle morphology of UMC lines grown alone (Mel270, OMM2.3) or co-cultured with LX-2 cells (Mel270/LX-2, OMM2.3/LX-2) for 48 hours. Scale bar, 50 µm. **B.** A volcano plot demonstrating differentially expressed transcripts in Mel270 and OMM2.3 cell lines grown alone. Transcripts listed in the volcano plot were selected on the basis of the significance for their differential expression in Mel270 cells versus OMM2.3 cells (horizontal dotted lines; $P<0.01$) and the level of induction or repression (vertical dotted lines; fold change>1.5). Total RNA was extracted after 48 hours and subjected to microarray analysis. **C.** Supernatants were collected after 48 hours from UMC lines grown alone, and the secretion of cytokines IL1β, IL6, IL6ST, IL8 and VEGFA was analyzed by ELISA. *$P<0.05$.
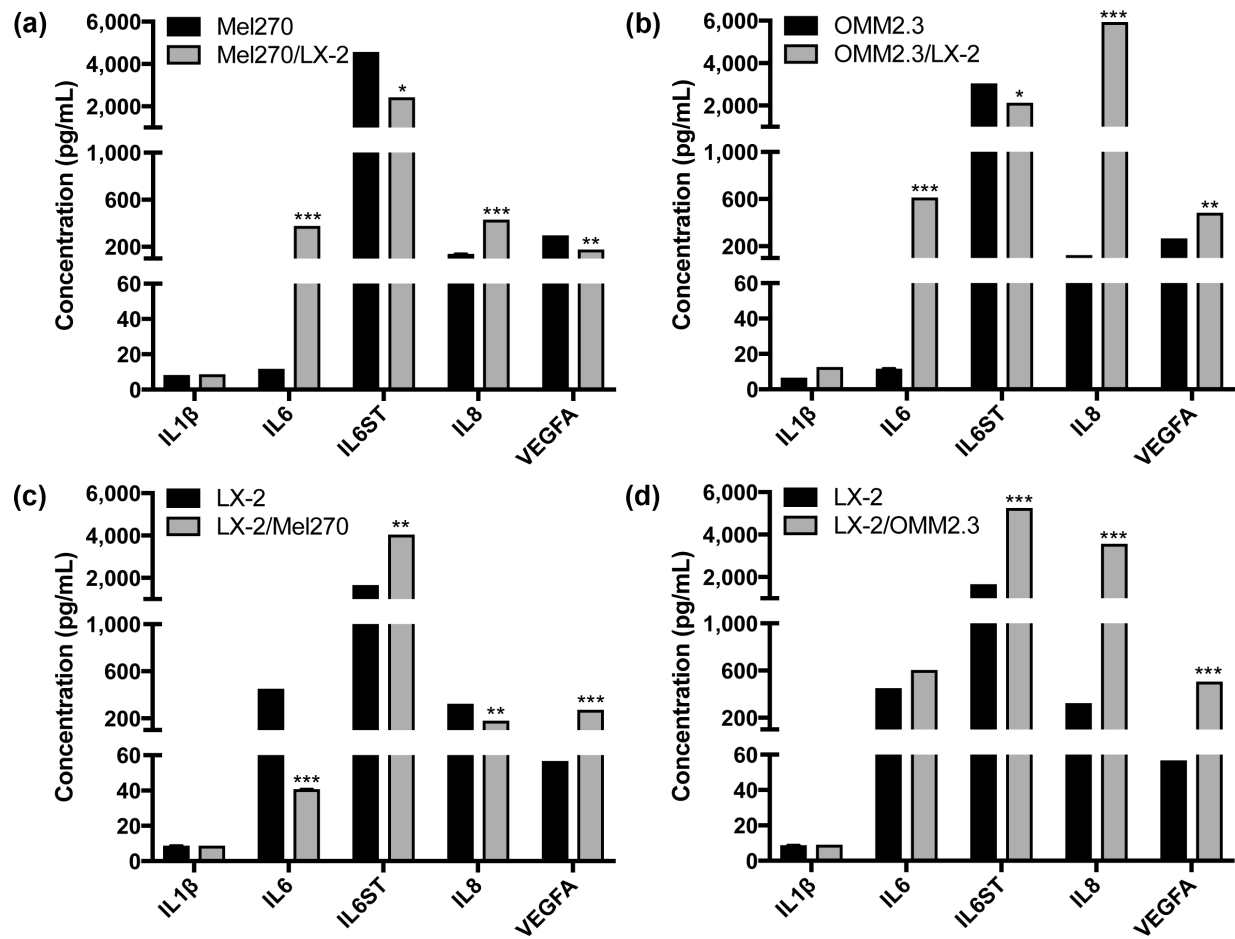
Suppl. Fig. 4. Proportional Venn diagrams representing the overlap of upregulated (**A** and **B**) or downregulated (**C** and **D**) transcripts in co-culture conditions. **A.** OMM2.3 (white) and Mel270 (black) were grown alone or co-cultured with LX-2 cells. **B.** LX-2 cells were grown alone or co-cultured with OMM2.3 (white) or Mel270 (black) cells. **C.** OMM2.3 (white) and Mel270 (black) were grown alone or co-cultured with LX-2 cells. **D.** LX-2 cells were grown alone or co-cultured with OMM2.3 (white) or Mel270 (black) cells. Transcripts listed in **A** to **D** were selected on the basis of the significance for their differential expression in monoculture versus co-culture conditions. Total RNA was extracted after 48 hours and subjected to microarray analysis.
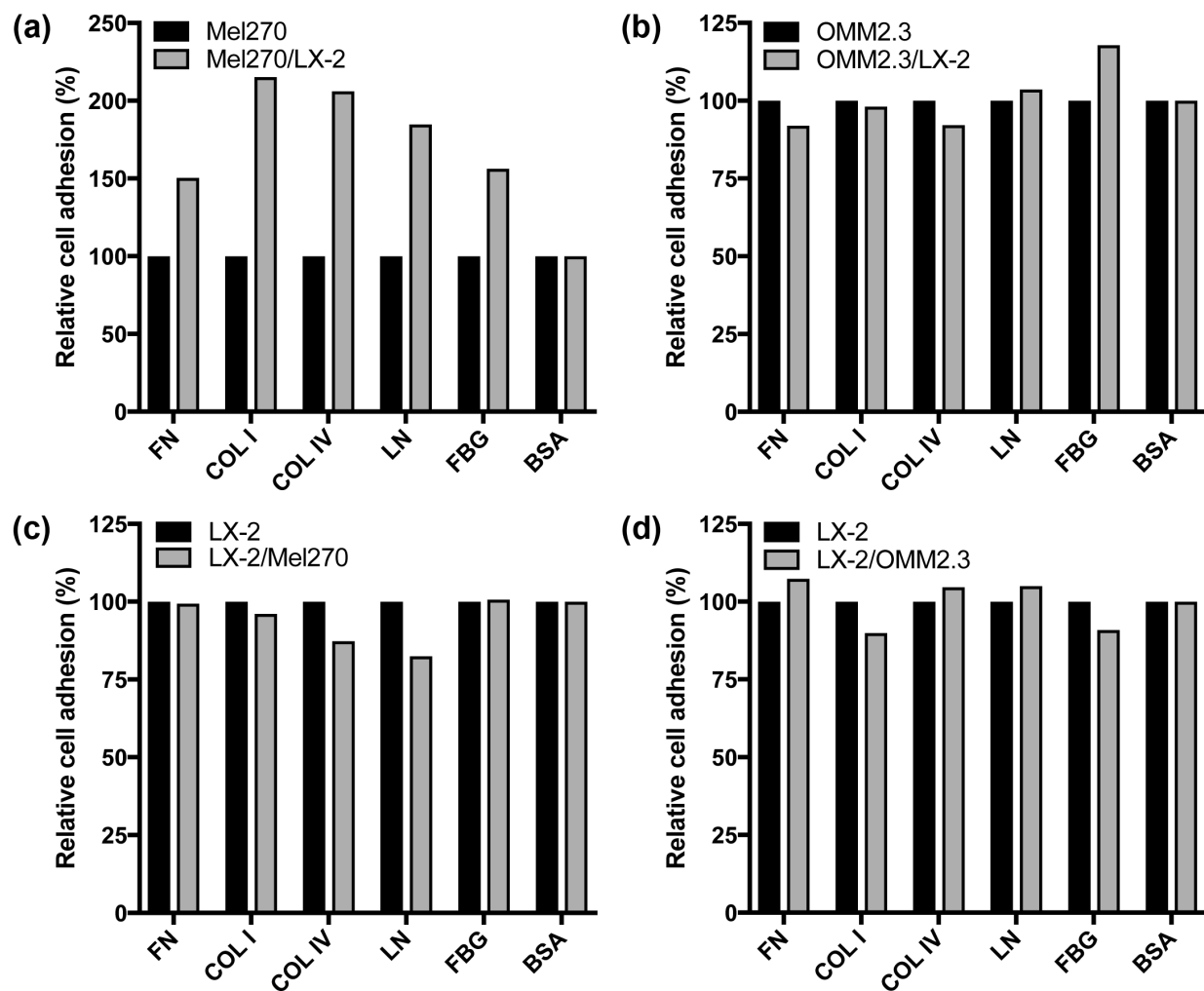
Suppl. Fig. 5. Quantitative analysis of the expression of integrin transcripts in co-cultures of UMCs and HSCs. **A.** Heatmap of the relative expression of alpha and beta integrin subunits in LX-2 cells and UMCs grown alone or in co-culture. The quantification is presented as percentage of relative expression in grayscale, where the largest value appears in black (100%), and the smallest value in white (0%). **B.** LX-2 cells were grown alone or in co-culture with UMCs (LX-2/Mel270, LX-2/OMM2.3). **C.** Mel270 and OMM2.3 cells were grown alone or co-cultured with HSCs (Mel270/LX-2, OMM2.3/LX-2). Total RNA was harvested after 48 hours and the expression of integrins ITGA1, ITGA3, ITGA4, ITGA5, ITGA10, ITGAX, ITGB2, ITGB3, ITGB4 and ITGB8 was analyzed by microarray. Fold change >2.00* or <0.50**.
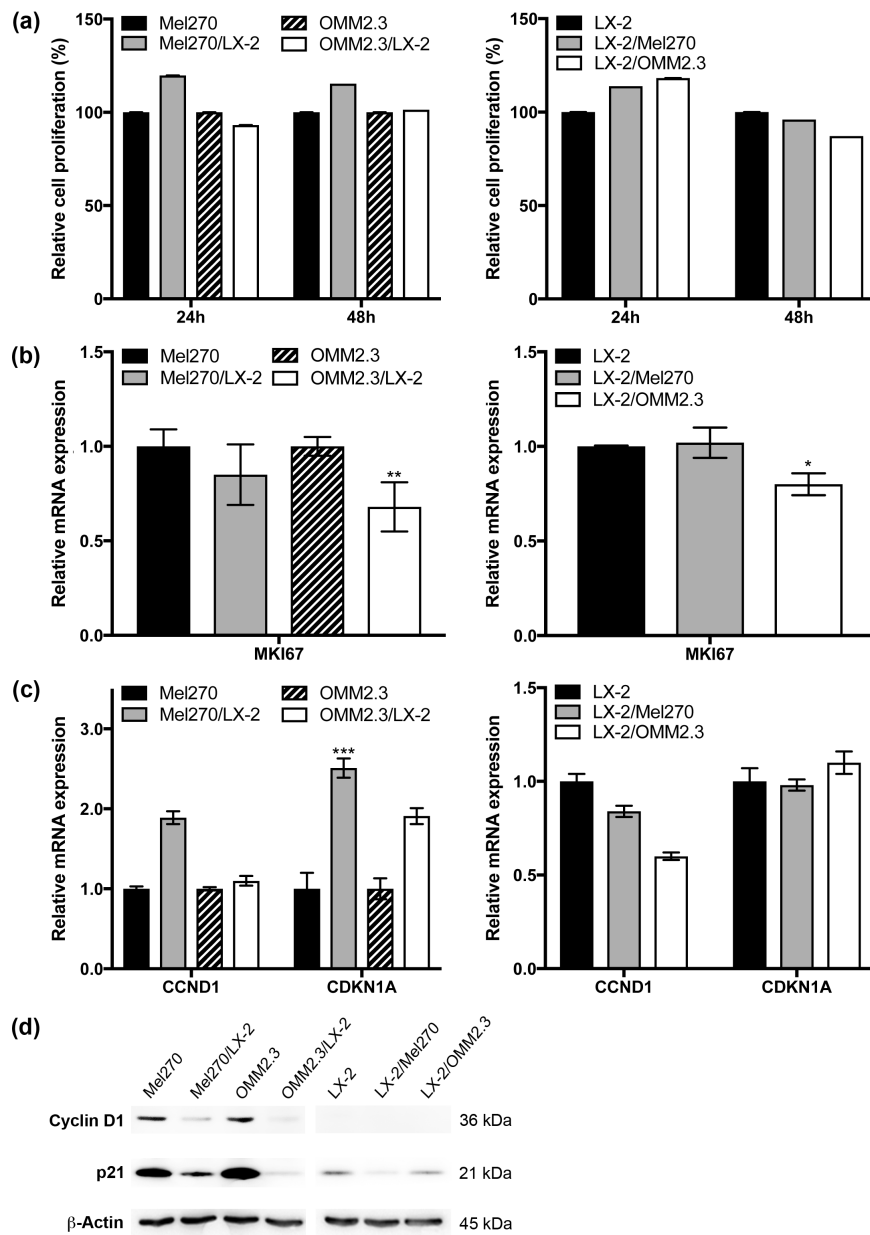
Suppl. Fig. 6. Effect of TCZ on STAT3 expression/activation and proliferation of UMC lines. **A.** Total proteins from Mel270, OMM2.3, and LX-2 cells grown alone or in co-culture conditions (Mel270/LX-2, OMM2.3/LX-2, LX-2/Mel270, LX-2/OMM2.3) and treated with TCZ were harvested after 48 hours. The expression of phosphor-STAT3 and total STAT3 was quantified by Western blotting (β-Actin, control loading). **B-D.** Cell proliferation was measured 48 hours post-TCZ treatment using the MTT colorimetric assays. **E-H.** Total RNA from Mel270, OMM2.3 and LX-2 cells grown alone or in co-culture conditions (Mel270/LX-2, OMM2.3/LX-2, LX-2/Mel270, LX-2/OMM2.3) treated with TCZ was harvested after 48 hours. The expression of the STAT3 transcript was analyzed by QPCR. *$P<0.05$, **$P<0.01$, ***$P<0.001$.

(a)

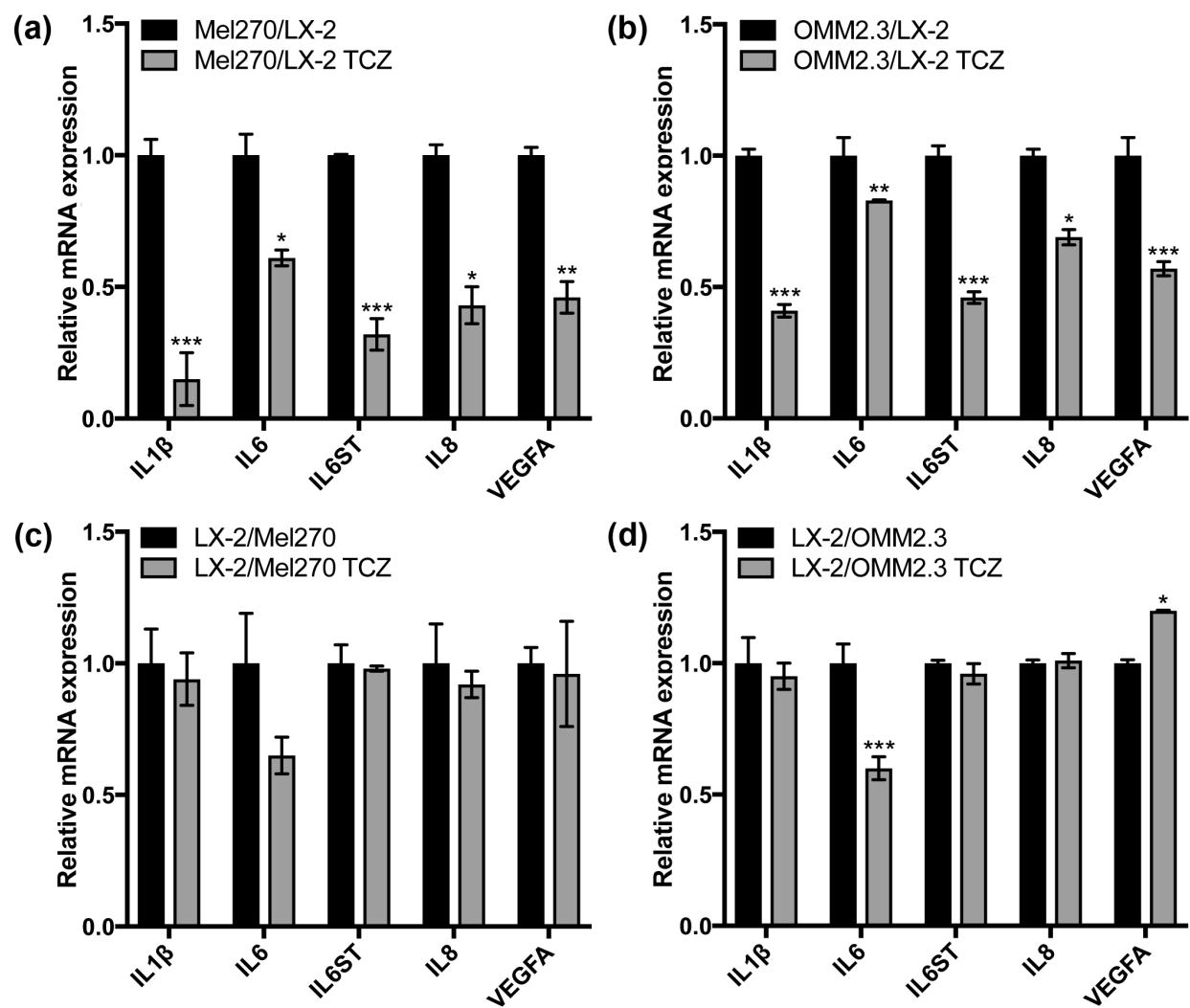**(b)**

(c)

(d)

Highlights

- Uveal melanoma is peculiar for its high propensity to spread to the liver
- Stellate cells are the most reactive cells of the liver in presence of metastases
- Metastatic cells are more sensitive to the paracrine signaling of stellate cells
- Inflammatory mediators are key players in the homing of uveal melanoma to the liver